




## Electron-electron interaction correction to the skew scattering contribution to the anomalous Hall effect in ultrathin FeCo films

Pengju Wang , Peng Chen, Yongzuo Wang, Yu Miao, and Cunxu Gao <sup>\*</sup>  
 Key Laboratory for Magnetism and Magnetic Materials of the Ministry of Education,  
 Lanzhou University, 730000 Lanzhou, People's Republic of China

 (Received 7 December 2023; revised 25 March 2024; accepted 1 April 2024; published 19 April 2024)

Electron-electron interaction (EEI), a quantum effect that occurs in low-dimensional or disordered systems at low temperatures, is an important issue in electron transport phenomena, especially in the anomalous Hall effect (AHE). Nevertheless, the role of EEI correction to the AHE is overlooked in conventional magnetic metal systems and the scaling exponents of the power-law fits are not consistently at the systems with sufficiently high disorder. Here, we demonstrate that EEI does correct to the AHE and cause  $\ln T$ -type temperature dependence of sheet resistance  $R_{xx}$  (conductance  $G_{xx}$ ), anomalous Hall resistance  $R_{AH}$ , and anomalous Hall conductance  $G_{AH}$  in ultrathin high-quality FeCo films in the low-temperature region. Furthermore, the scaling exponent  $\gamma \sim 1$  is acquired through the power-law fits of  $G_{AH} \sim G_{xx}^\gamma$  by varying temperature or thickness, suggesting that EEI corrects to skew scattering and definitely results in skew scattering dominating AHE in the bad metal regime ( $\sigma_{xx} < 1 \times 10^4$  S/cm).

DOI: [10.1103/PhysRevB.109.144416](https://doi.org/10.1103/PhysRevB.109.144416)

### I. INTRODUCTION

The anomalous Hall effect (AHE) is a remarkable topic in condensed matter physics that exists in systems with broken time-reversal symmetry [1,2]. In particular, the AHE occurs in ferromagnetic metals as a consequence of spin-orbit coupling (SOC) [1,3–7]. It is generally accepted that the AHE originates from three different mechanisms: skew scattering, side jump, and an intrinsic mechanism, i.e., anomalous Hall (AH) conductivity,  $\sigma_{AH} \cong \sigma_{AH}^{sk} + \sigma_{AH}^{sj} + \sigma_{AH}^{in}$  (conductance  $G_{AH} \cong G_{AH}^{sk} + G_{AH}^{sj} + G_{AH}^{in}$ ) [1]. The skew scattering is derived from considering an asymmetric scattering from impurity with SOC, which is proportional to the transport relaxation time  $\tau$  and gives  $G_{AH}^{sk} \propto \tau^1 \propto G_{xx}^1$  ( $G_{xx}$  is the sheet conductance) [4,5]. The side jump is a sudden displacement of conduction electrons scattered by impurity potentials in the presence of SOC [6]. The intrinsic mechanism, however, arises from the transverse velocity of spin-polarized conduction electrons induced by SOC and interband mixing [3]. Significantly, this mechanism could be associated with the integral of all the Berry curvatures over the whole Brillouin zone [8,9]. In contrast to skew scattering, both the side jump and the intrinsic mechanism are independent of  $\tau$ , and yield  $G_{AH}^{sj}$  ( $G_{AH}^{in}$ )  $\propto \tau^0 \propto G_{xx}^0$  [1,6,9].

A significant issue in the AHE is the quantum correction from weak localization (WL) and/or electron-electron interaction (EEI) in the systems with lower dimensionality and/or strong disorder strength at sufficiently low temperatures [1,10–14]. Bergmann and Ye [15] first showed that the AH conductivity was independent of temperature at low temperatures in ultrathin amorphous Fe films, despite that

$\ln T$ -type dependence on sheet and AH resistances was found. They proposed that the EEI correction to the AHE vanished while the WL correction was suppressed by magnetic scattering. The results were further supported by Langenfeld and Wölfle, and they proposed that Coulomb anomaly terms due to Altshuler-Aronov corrections cancel identically from the anomalous Hall conductivity by an explicit calculation [16]. Then the early theoretical calculations pointed out that the EEI correction to the AHE disappeared for general symmetry reasons (the presence of mirror symmetry) [17]. Conversely, the WL correction to the side jump is absent, but that to the skew scattering is nonzero [18]. The observed quantum corrections to the AHE at low temperatures were spontaneously attributed to WL in subsequent experimental works, such as in Fe [19,20], Ni [21], FePt [22], and CoFeB films [23].

In contrast to WL, the EEI correction to the AHE was only experimentally reported in  $\text{CNi}_3$  films [24] and  $n$ -type  $\text{HgCr}_2\text{Se}_4$  crystals [25], and was associated with the density of states (DOS) near the Fermi energy and possible mirror symmetry breaking, respectively. Recently, Li and Levchenko [26,27] theoretically suggested that the EEI in the Cooper channel can cause a temperature-dependent correction to the AHE even for nonsuperconducting materials, which should account for the case in  $\text{HgCr}_2\text{Se}_4$ . So far, it remains unclear whether the EEI corrects to the AHE or not in conventional magnetic metal systems. The theoretical calculation indicates the EEI correction mainly comprises the contribution of Maki-Thompson (MT) and DOS terms [26–31]. Both MT [29,31] and DOS [30] terms contribute to skew scattering; nevertheless, the side jump only exists in the DOS contributions [26,27,32]. Based on the different dependence of  $G_{AH}^{sk}$  and  $G_{AH}^{sj}$  on  $G_{xx}$ , the AHE in the systems with EEI correction was scaled by the power-law fits of  $G_{AH} \sim G_{xx}^\gamma$ , and various values of  $\gamma$  ( $\geq 2$ ) were observed [24,25]. However, these

<sup>\*</sup>Corresponding author: [gaocunx@lzu.edu.cn](mailto:gaocunx@lzu.edu.cn)

results diverge from not only the relations of  $G_{AH}^{sk} \propto G_{xx}^1$  (skew scattering) and  $G_{AH}^{sj} \propto G_{xx}^0$  (side jump), but also the universal scaling relation of  $G_{AH} \propto G_{xx}^{1.6}$  in the bad metal regime ( $\sigma_{xx} < 1 \times 10^4$  S/cm) [1,33–35]. Therefore, it is necessary to determine whether the EEI correction to skew scattering or side jump dominates the AHE in the low-temperature region.

In the present work, we report a  $\ln T$ -type EEI correction to the AHE in ultrathin high-quality FeCo films. The WL is excluded by analyzing the temperature dependence of sheet conductance  $G_{xx}$  and the nearly constant values of  $dG_{xx}/d\ln T$  under different magnetic fields. The EEI correction to the AHE has been identified using Bergmann and Ye's notation. Furthermore, the skew scattering dominating the AHE is determined by the power-law fits of  $G_{AH} \sim G_{xx}^\gamma$  ( $\gamma \sim 1$ ) as varying temperature or thickness, suggesting that the EEI mainly corrects to skew scattering at low temperatures.

## II. EXPERIMENT

The epitaxial FeCo films with thickness varying from 1.0 to 3.0 nm were grown on MgO(001) substrates in a custom-built molecular beam epitaxy (MBE) system. The sample growth conditions are consistent with our previous work [36]. Nucleation and growth were monitored *in situ* by reflection high-energy electron diffraction (RHEED). The crystal structure and orientation of the films were assessed by high-resolution x-ray diffractometry (HRXRD) (X'Pert<sup>3</sup> MRD, PANalytical, Netherlands). The transport measurements were performed on a physical property measurement system (PPMS, Quantum Design Inc., San Diego, CA) by a standard four-probe method with the current applied along the MgO[100] direction.

## III. RESULTS AND DISCUSSION

The surface morphology and crystal quality of FeCo films are first elucidated. The RHEED patterns of the MgO(001) substrates and FeCo film surfaces were taken along different orientations before and after film growth, respectively. Figures 1(a) and 1(b) display the stationary RHEED patterns of the MgO(001) surface taken along the  $\langle 100 \rangle$  and  $\langle 110 \rangle$  azimuths prior to FeCo growth, respectively. The insulating nature of the MgO(001) substrate leads to the fuzzy distorted pattern by substrate charging. Figures 1(c) and 1(d) [Figs. 1(e) and 1(f)] show the RHEED patterns of the FeCo surface taken along the  $\langle 100 \rangle$  and  $\langle 110 \rangle$  azimuths of MgO, respectively, with FeCo films grown to a thickness of 1.0 (3.0) nm. A series of distinct streaks is observed even for 1.0-nm FeCo films. The results indicate that the FeCo films exhibit a smooth single-crystal surface and the electrons are reflected from the surface. In this reflection mode, the incident electrons only penetrate the very top atomic layer and the reciprocal lattice rods would become narrow streaks [37]. The traditional geometrical lattice matching theory allows us to assert an expected orientation relationship of body-centered cubic (bcc) FeCo(001)  $\langle 110 \rangle \parallel$  MgO(001)  $\langle 100 \rangle$ .

The HRXRD measurements are performed for the FeCo films. Figures 2(a) and 2(b) show symmetric and asymmetric HRXRD spectra for 1.0–3.0-nm FeCo films grown on

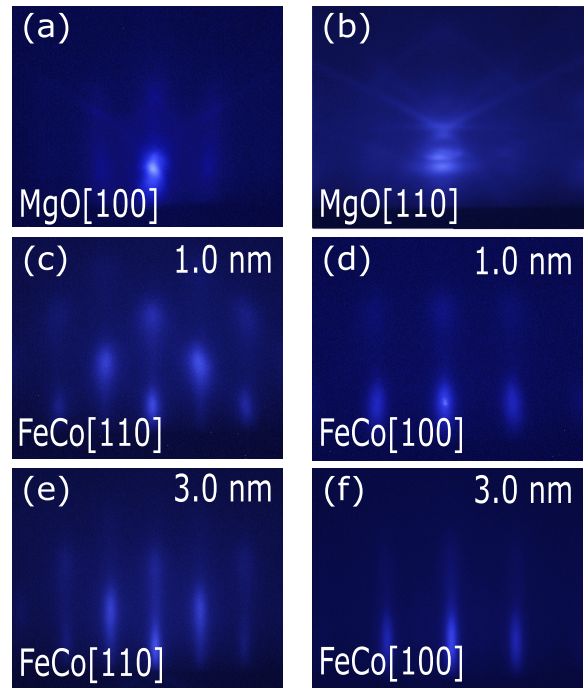


FIG. 1. Surface morphology of FeCo films. RHEED patterns of the MgO(001) and FeCo surfaces taken along azimuths (a) MgO[100], (b) MgO[110], (c) 1.0-nm FeCo[110], (d) 1.0-nm FeCo[100], (e) 3.0-nm FeCo[110], and (f) 3.0-nm FeCo[100], respectively.

MgO(001), respectively. As the film thickness  $d$  increases, the diffraction peak of FeCo(002) planes around  $2\theta = 66.3^\circ$  occurs at  $d = 1.3$  nm ( $\sim 9$  monolayers). The peak is apparent at  $d = 2.0$  nm ( $\sim 14$  monolayers). These results testify to the formation of bcc structure, and the out-of-plane lattice parameter is about 2.82 Å [38]. Compared with the thick film, the lattice parameter is about 1% smaller, which should be attributed to the epitaxial stress [36]. On the other hand, the unambiguous FeCo(101) diffraction peak is recognized at a thickness of only 1 nm ( $\sim 7$  monolayers). These results demonstrate the excellent crystal quality of FeCo films. Figure 2(c) shows the  $\phi$  scans of the MgO(202) and FeCo(101) planes of the 3-nm FeCo films. The  $90^\circ$ -interval reflections indicate an in-plane fourfold symmetry. A relative  $45^\circ$  rotation of the FeCo films with respect to the MgO substrate is observed, revealing the epitaxial growth of the films. This is corresponding to the RHEED results shown in Fig. 1. Figure 2(d) exhibits the residual resistivity  $\rho_{xx0}$  [obtained by the conversion of Drude conductance  $G_0 (= 1/R_{xx0})$ ] [19], see below] as a function of thickness  $d$  for FeCo films. According to Matthiessen's rule [39,40],  $\rho_{xx0}$  results from static scattering by impurities and is temperature independent. The  $\rho_{xx0}$  increases and represents a sixfold change with decreasing  $d$ , indicating the fact that surface scattering is dominant in the present FeCo films [19,41]. It is worth noting that  $\rho_{xx0}$  decreases continuously as  $d$  increases for varying  $d$  from 1.0 to 43.8 nm, as shown in inset in Fig. 2(d). This suggests that the density of impurities is controlled by the film thickness  $d$ , which is analogous to doping layers of impurities to the bulk single-crystal FeCo

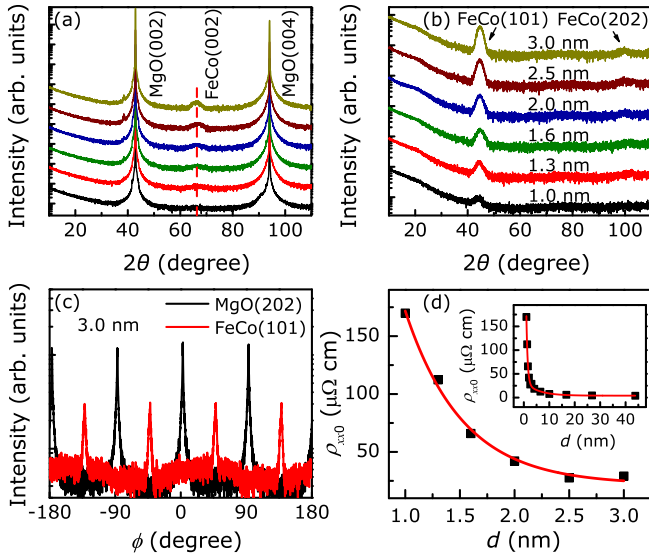


FIG. 2. Crystal quality and surface scattering of FeCo films. (a) Symmetric and (b) asymmetric HRXRD spectra for 1.0–3.0-nm FeCo films. (c) HRXRD azimuthal  $\phi$  scans of the bcc FeCo(101) and MgO(202) planes for 3.0-nm FeCo films. (d) Thickness  $d$  dependence of the residual resistivity  $\rho_{xx0}$  for 1.0–3.0-nm FeCo films. Inset: The  $\rho_{xx0}$  as a function of  $d$  for 1.0–43.8-nm FeCo films. Note that the data of 4.1–43.8-nm FeCo films are obtained from our previous work [36]. The red lines are a guide for the eye.

alloys [36,41,42]. When the density of layers is relatively high (i.e., the film thickness  $d$  is small), the electrical transport phenomenon may be affected by quantum effects such as WL and/or EEI at sufficiently low temperatures [10–13].

The low-temperature electronic transport properties of FeCo films are then measured. Figures 3(a) and 3(b) show the normalized sheet resistance  $R_{xx}$  and AH resistance  $R_{AH}$  as a function of temperature  $T$  for FeCo films with different thickness, respectively. Evidently, the  $R_{xx}$  shows an insulating behavior for 1.0–3.0-nm FeCo films in the low-temperature region, i.e.,  $dR_{xx}/dT < 0$ . Except for 1.0-nm FeCo films, all the other films exhibit metallic  $R_{xx}$  ( $dR_{xx}/dT > 0$ ) at high temperatures. The minimum values of  $R_{xx}$  correspond to  $T_{\min} = 140, 60, 35, 25,$  and  $20$  K for 1.3-, 1.6-, 2.0-, 2.5-, and 3.0-nm FeCo films, respectively. The increase in  $R_{xx}$  for  $T < T_{\min}$  can be attributed to the quantum correction of WL and/or EEI to Drude resistance [13].

In a two-dimensional (2D) or quasi-two-dimensional system, the temperature dependence of sheet conductance  $G_{xx}$  ( $= 1/R_{xx}$ ) can be expressed as [11,13,22,43]

$$G_{xx}(T) = G_0 + p \frac{e^2}{\pi h} \ln\left(\frac{T}{T_0}\right) + (1-F) \frac{e^2}{\pi h} \ln\left(\frac{T}{T_0}\right), \quad (1)$$

where  $G_0$  is Drude conductance, and the second and third terms on the right-hand side stand for the correction of WL and EEI, respectively. Herein,  $p$  is a temperature exponent with  $0 \leq F \leq 1$ . Note that the value of  $p$  is determined by inelastic relaxation mechanisms:  $p = 1$  for electron-electron scattering and  $p = 2/3$  for electron-phonon scattering (depending on the material and temperature) [13]. According to

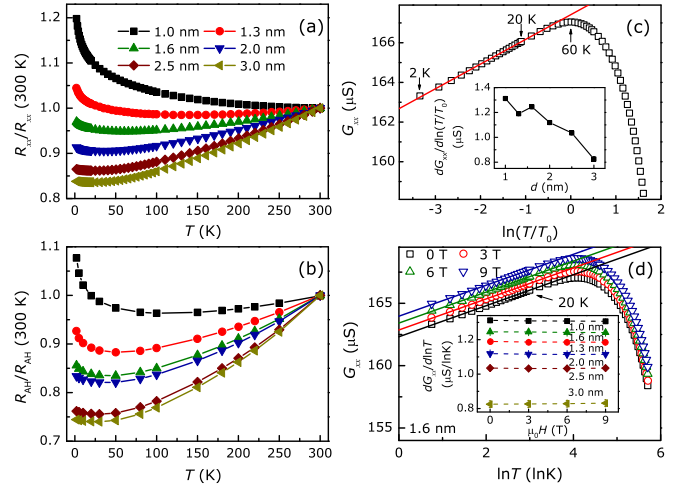


FIG. 3. Quantum corrections to sheet resistance and AH resistance. [(a), (b)] Temperature dependence of the normalized sheet resistance  $R_{xx}$  and anomalous Hall resistance  $R_{AH}$  for FeCo films with various thicknesses, respectively. (c)  $G_{xx}$  as a function of  $\ln(T/T_0)$  for 1.6-nm FeCo films.  $T_0$  is taken as 60 K, which corresponds to the conductance maximum. The red line is the linear fit according to Eq. (1), and the dependence of  $dG_{xx}/d\ln(T/T_0)$  on thickness  $d$  of FeCo films is shown in inset. (d)  $G_{xx}$  as a function of  $\ln T$  for 1.6-nm FeCo films in magnetic fields (0, 3, 6, and 9 T). The inset shows  $dG_{xx}/d\ln T$  as a function of magnetic field for FeCo films with different thickness.

Eq. (1), the  $G_{xx}$  as a function of  $\ln(T/T_0)$  for 1.6-nm FeCo films is shown in Fig. 3(c), for instance. A perfect linear fit for the data between 2 and 20 K is observed, consistent with the validity of the 2D assumption [11,13,22]. Here,  $T_0$  is the temperature corresponding to  $T_{\min} = 60$  K for 1.6-nm FeCo films. The derived  $dG_{xx}/d\ln(T/T_0)$  as a function of thickness  $d$  is presented in the inset of Fig. 3(c). As  $d$  increases,  $dG_{xx}/d\ln(T/T_0)$  generally decreases, indicating the decline of quantum correction to sheet conductance  $G_{xx}$ . It is worth noting that the value of  $dG_{xx}/d\ln(T/T_0)$  is on the order of  $1 \times 10^{-6}$  S and one order smaller than  $e^2/\pi h$  ( $1.233 \times 10^{-5}$  S), suggesting that  $p + (1-F) \sim 0.1$ . Considering that  $p$  is an integer and  $p > 0$  if a system exhibits a quantum correction from WL [11,13],  $p = 0$  can be distinctly determined. The result manifests that the WL correction to  $G_{xx}$  is negligible and only EEI provides a correction to  $G_{xx}$  in FeCo films in the low-temperature region. In fact,  $p + 1 - (F) \sim 1$  was shown in FePt [22], Fe [15,20], and CoFeB films [23], because only WL exists in these systems. It was also reported that  $p + 1 - (F) < 1$  in polycrystalline systems with WL correction ( $1 - F = 0$ ), such as Fe [20] and Ni films [21], which was attributed to the intergranular tunneling effect using the granular model. Conversely, for polycrystalline systems with EEI correction ( $p = 0$ ), the intergrain-type EEI correction may cause  $p + (1-F) > 1$  ( $F < 0$ ), such as in the case of polycrystalline Sn-doped indium oxide films. For a single-crystalline system, however, the intergranular effect was absent and conventional EEI theory (Altshuler-Aronov type) gives rise to  $p + (1-F) < 1$  ( $p = 0$  and  $F > 0$ ) [44]. Furthermore, the values of  $F$  increase as film thickness increases, which is similar to the dependence of  $dG_{xx}/d\ln(T/T_0)$  [ $= p + (1-F)$ ]

decreasing with increasing  $d$  shown in the inset of Fig. 3(c) [44]. These results reveal the absence of the intergranular effect in present FeCo films. This can be attributed to the excellent crystal quality and surface morphology of these samples (Figs. 1 and 2).

Furthermore, one can exclude the WL correction to  $G_{xx}$  by the nearly constant values of  $dG_{xx}/d\ln T$  under magnetic fields (on the order of tesla or less), because the WL is usually suppressed in a strong magnetic field [11,25,45]. Figure 3(d) displays the dependence of the sheet conductance  $G_{xx}$  on  $\ln T$  for 1.6-nm FeCo films in magnetic fields from zero to  $\mu_0 H = 9$  T. It is evident that  $G_{xx}$  has a linear dependence on  $\ln T$  in the temperature range 2–20 K. The values of  $dG_{xx}/d\ln T$  as a function of magnetic field for FeCo films with different thickness are shown in the inset of Fig. 3(d). The nearly constant values of  $dG_{xx}/d\ln T$  clearly demonstrate the irrelevance of WL in present FeCo films. These results further confirm that only EEI provides a correction to  $G_{xx}$ .

Now we turn to explore the EEI correction to AH conductance  $G_{AH} [=R_{AH}/(R_{AH}^2 + R_{xx}^2)]$  in the low-temperature region (2–20 K). It is observed that the AH resistance  $R_{AH}$  and conductance  $G_{AH}$  have logarithmic temperature dependence (see Sec. 1 and Fig. S1 in the Supplemental Material [46]). According to Bergmann and Ye's notation [16], the normalized relative changes  $\Delta^N R_{xx}$ ,  $\Delta^N R_{AH}$ , and  $\Delta^N G_{AH}$  can be used to represent quantum corrections to  $R_{xx}$ ,  $R_{AH}$ , and  $G_{AH}$ , respectively. Here, the normalized relative change is defined as  $\Delta^N Q_{ij} = [\pi h / (e^2 R_0) (\delta Q_{ij} / Q_{ij})]$  with  $\delta Q_{ij} = Q_{ij}(T) - Q_{ij}(2 \text{ K})$  and  $R_0 = R_{xx}(2 \text{ K})$  [20]. For all FeCo films,  $|\delta R_{xx}| \ll R_0$  and  $R_{AH}(T) \ll R_{xx}(T)$ , so that  $\Delta^N R_{xx}$ ,  $\Delta^N R_{AH}$ , and  $\Delta^N G_{AH}$  can be expressed as

$$\Delta^N R_{xx} = \left( \frac{\pi h}{e^2} \frac{1}{R_0} \right) \left( \frac{\delta R_{xx}}{R_{xx}} \right) = -A_R \ln \left( \frac{T}{T_0} \right), \quad (2a)$$

$$\Delta^N R_{AH} = \left( \frac{\pi h}{e^2} \frac{1}{R_0} \right) \left( \frac{\delta R_{AH}}{R_{AH}} \right) = -A_{AH} \ln \left( \frac{T}{T_0} \right) \quad (2b)$$

and

$$\Delta^N G_{AH} = \left( \frac{\pi h}{e^2} \frac{1}{R_0} \right) \left( \frac{\delta G_{AH}}{G_{AH}} \right) = -A_G \ln \left( \frac{T}{T_0} \right), \quad (2c)$$

respectively. In fact,  $A_G = 2A_R - A_{AH}$  can be deduced by the above equations, and if  $A_G \neq 0$  then the quantum correction does contribute to the AH conductance  $G_{AH}$  [16,20,22].

$\Delta^N R_{xx}$ ,  $\Delta^N R_{AH}$ , and  $\Delta^N G_{AH}$  as functions of  $\ln T$  for 1.6-nm FeCo films are shown in Fig. 4(a), for example. It is evident that  $\Delta^N Q_{ij}$  fits well linearly with  $\ln T$  at 2–20 K, and the prefactors  $A_R = 0.1012$ ,  $A_{AH} = 0.135$ , and  $A_G = 0.059$  can be derived based on Eqs. (2). Note that  $A_G$  is directly acquired from the fits using Eq. (2c). Figure 4(b) shows the prefactors as a function of thickness  $d$  for FeCo films with different thickness. The values of  $A_G$  are very close to  $2A_R - A_{AH}$  for all the films, revealing that the fits are accurate for all samples. What is prominent is that  $A_G$  is obviously greater than zero for 1.0–1.6-nm FeCo films, indicating that the EEI correction to  $G_{AH}$  is nonzero [15,20,22]. This is unusual because EEI is generally believed to be uncorrected for both skew scattering and side jump for general symmetry reasons [16,17]. It had only been reported that EEI corrected to AHE in ultrathin  $\text{CNi}_3$  films [24] and  $n$ -type  $\text{HgCr}_2\text{Se}_4$

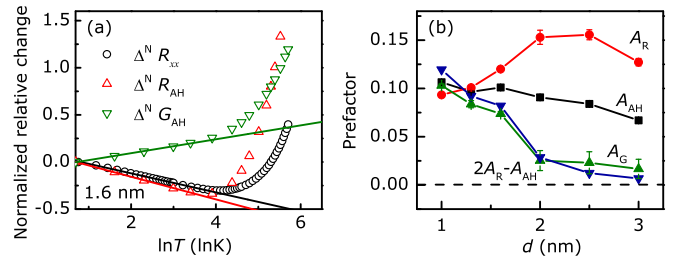


FIG. 4. EEI correction to AH conductance. (a)  $\ln T$  dependence of normalized relative changes in the sheet resistance  $R_{xx}$ , anomalous Hall resistance  $R_{AH}$ , and anomalous Hall conductance  $G_{AH}$  for 1.6-nm FeCo films. The straight lines are the linear fits to the data from 2 to 20 K. (b) Prefactors  $A_R$ ,  $A_{AH}$ ,  $A_G$ , and  $2A_R - A_{AH}$  as a function of thickness  $d$  for FeCo films.

[25], and was associated with the DOS near the Fermi energy and possible mirror symmetry breaking, respectively. Recently, Li and Levchenko [26] proposed that EEI in the Cooper channel produces temperature-dependent corrections to the AH conductivity even for nominally nonsuperconducting materials at low temperatures, and may provide a possible explanation for the unconventional temperature dependence of the AHE in  $\text{HgCr}_2\text{Se}_4$ . Consequently, the EEI correction to the AHE in ultrathin FeCo films may be attributed to the electron interactions in the Cooper channel [26]. In addition, the value of  $A_G$  decreases as  $d$  increases from 1.0 to 1.6 nm, maybe due to the reduction of the disorder strength for FeCo films [25]. According to the 2D localization theory, the disorder strength can be represented by disorder parameter  $k_F l$ , and strong disorder strength corresponds to small  $k_F l$  [22,47]. The value of  $k_F l$  can be calculated from the  $R_{xx}$  using  $k_F l = (h/e^2)/R_{xx} = G_{xx}/(e^2/h)$  in a 2D system, where  $k_F$  is the Fermi wave number,  $l$  is the elastic mean free path, and  $h/e^2$  is the quantum resistance [13,47]. As  $d$  decreases from 1.6 to 1.0 nm,  $k_F l$  of FeCo films decreases from 4.2 to 0.88 at 2 K. Significantly,  $k_F l = 0.88$  for 1.0-nm FeCo films is lower than the Ioffe-Regel limit ( $k_F l \sim 1$ ). Even so,  $G_{xx}$ ,  $R_{AH}$ , and  $G_{AH}$  show a linear dependence on  $\ln T$  at 2–20 K (Fig. 3 and Fig. S1 in the Supplemental Material [46]), which follows the characteristic behavior in a weakly localized regime [13]. This is different from the case in polycrystalline  $\text{CNi}_3$  films and FePt films, in which  $G_{xx}$  (or  $R_{xx}$ ) depends on  $T^{1/2}$  (or  $T^{-1/3}$ ) for samples with  $k_F l < 1$  [22,24]. The results may be because impurity scattering is dominated by surface scattering in FeCo films, which benefits from the excellent crystal quality and surface morphology. Up to  $d > 2.0$  nm, the  $A_G$  is close to zero and does not change with  $d$ , indicating that EEI correction to  $G_{AH}$  is negligible for 2.0–3.0-nm FeCo films. This finding corresponds to the transport character in a weakly disordered regime ( $k_F l \gg 1$ ).

To expose the evolution of the AHE with varying temperature  $T$  and to scale the AHE for 1.0–1.6-nm FeCo films, log-log plots of the AH resistance  $R_{AH}$  (conductance  $G_{AH}$ ) as a function of the sheet resistance  $R_{xx}$  (conductance  $G_{xx}$ ) are shown in Fig. 5. Note that the data are discussed under the resistance and conductance representation because of the 2D nature of the transport [24]. Here,  $R_Q = h/e^2$  stands for the quantum resistance. The good linear depen-

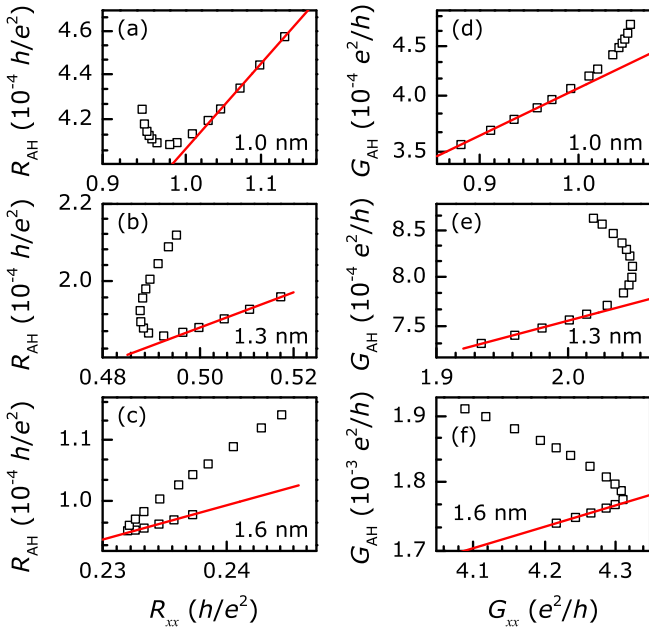


FIG. 5. Scaling of AHE by varying temperature. [(a)–(c)] Log-log plot of the anomalous Hall resistance  $R_{\text{AH}}$  of 1.0-, 1.3-, and 1.6-nm FeCo films as a function of the sheet resistance  $R_{\text{xx}}$  with varying temperature.  $R_{\text{Q}} = h/e^2$  is the quantum resistance. The solid lines provide a guide for the eye. [(d)–(f)] Log-log plot of the anomalous Hall conductance  $G_{\text{AH}}$  of 1.0-, 1.3-, and 1.6-nm FeCo films as a function of the sheet conductance  $G_{\text{xx}}$  with varying temperature. The solid lines are the separate power-law fits to the data from 2 to 20 K.

dence of  $R_{\text{AH}}$  on  $R_{\text{xx}}$  at a temperature range of 2–20 K for 1.0–1.6-nm FeCo films is apparent in Figs. 5(a)–5(c). The power-law fits of  $G_{\text{AH}} \sim G_{\text{xx}}^{\gamma}$  (2–20 K) in Figs. 5(d)–5(f) derive the exponents  $\gamma = 1.07 \pm 0.01$ ,  $\gamma = 0.89 \pm 0.03$ , and  $\gamma = 0.74 \pm 0.01$  for 1.0-, 1.3-, and 1.6-nm FeCo films, respectively. It is well known that the AHE originated from three different mechanisms: skew scattering, the side jump, and an intrinsic mechanism ( $G_{\text{AH}} \cong G_{\text{AH}}^{\text{sk}} + G_{\text{AH}}^{\text{sj}} + G_{\text{AH}}^{\text{sk}}$ ) [1]. These mechanisms yield diverse dependences of AH conductance  $G_{\text{AH}}$  on sheet conductance  $G_{\text{xx}}$ : skew scattering gives  $G_{\text{AH}} \sim G_{\text{xx}}^1$ , while the side jump and intrinsic mechanism give  $G_{\text{AH}} \sim G_{\text{xx}}^0$ . Therefore, the scaling exponent  $\gamma \sim 1$  for 1.0-nm FeCo films suggests that  $G_{\text{AH}}$  is completely dominated by the skew scattering. It manifests that the EEI mainly corrects to skew scattering and leads to the contribution of skew scattering dominating the AHE of 1.0-nm FeCo films in the low-temperature region. Interestingly, the values of  $\gamma$  decrease as  $d$  increases, indicating the reduced contribution of skew scattering and enhanced contribution of the side jump and/or intrinsic mechanism to AHE. Specifically, the disorder strength  $k_{\text{F}}l$  of FeCo films is reduced with increasing  $d$ , causing weakened EEI correction to skew scattering. Additionally, the contribution of the intrinsic mechanism to the AHE would increase due to the enhanced Berry curvature with increasing  $d$  [1,19]. It is also worth noting that the temperature-related side jump contribution cannot be ignored even in the low-temperature region in the present FeCo film system while varying  $T$  (see Sec. 2 and Fig. S2 in the Supplemental Material [46]) [36].

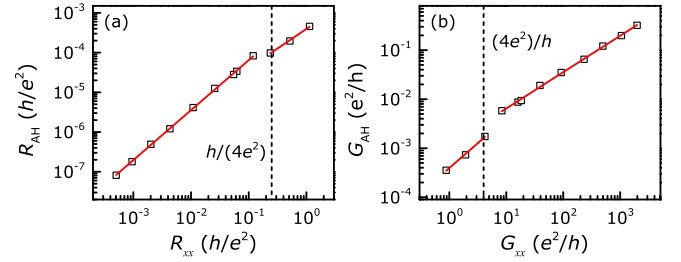


FIG. 6. Scaling of AHE by varying sample thickness. (a) Log-log plot of the anomalous Hall resistance  $R_{\text{AH}}$  of FeCo films as a function of the sheet resistance  $R_{\text{xx}}$  at 2 K. The solid lines provide a guide for the eye. (b) Log-log plot of the anomalous Hall conductance  $G_{\text{AH}}$  as a function of the sheet conductance  $G_{\text{xx}}$  at 2 K. The solid lines are separate power-law fits to the low- and high-conductance data, giving exponents of  $\gamma = 1.01 \pm 0.05$  and  $\gamma = 0.74 \pm 0.01$ , respectively. Note that the data of 4.1–43.8-nm FeCo films are obtained from our previous work [36].

Furthermore, the disorder strength of ultrathin films can be tuned by varying thickness in the low-temperature limit (2 K) [22,24]. The log-log plots of data at 2 K for FeCo films with different thickness  $d$  are performed in Fig. 6. Note that the data of 4.1–43.8-nm FeCo films are obtained from our previous work [36]. Figure 6(a) shows the AH resistance  $R_{\text{AH}}$  as a function of sheet resistance  $R_{\text{xx}}$  at 2 K. It is evident that  $R_{\text{AH}}$  changes almost linearly with  $R_{\text{xx}}$  for  $R_{\text{xx}} < h/(4.22e^2)$  and  $R_{\text{xx}} > h/(4.22e^2)$ , respectively. The result suggests that  $R_{\text{xx}} \sim h/(4.22e^2)$  is a crossover point in FeCo films. This crossover corresponds to a film thickness of  $d = 1.6$  nm, similar to the case of 2.0 nm in  $\text{CNi}_3$  films [24] and 3.0 nm in FePt films [22]. But the difference is that  $R_{\text{AH}}$  remains unsaturated as  $R_{\text{xx}}$  increases through the threshold of the metal-insulator transition for 1.0–3.0-nm FeCo films ( $k_{\text{F}}l \sim 0.88$ –18.3). The AH conductance  $G_{\text{AH}}$  as a function of sheet conductance  $G_{\text{xx}}$  at 2 K is displayed in Fig. 6(b). As  $G_{\text{xx}}$  increases for FeCo films with  $d = 1.0$ –1.6 nm, where  $G_{\text{AH}}$  is well demonstrated to receive an EEI correction, the scaling of  $G_{\text{AH}} \sim G_{\text{xx}}^{\gamma}$  yields an exponent  $\gamma = 1.01 \pm 0.05$ . Otherwise,  $\gamma = 0.74 \pm 0.01$  for FeCo films with  $G_{\text{xx}} > 4.22e^2/h$  ( $d = 2.0$ –43.8 nm) at 2 K. According to the scaling relations, the scaling exponent  $\gamma \sim 1$  suggests that  $G_{\text{AH}}$  is completely dominated by the skew scattering. It manifests that the EEI corrects to skew scattering of the AHE and leads to the contribution of skew scattering dominating the AHE for 1.0–1.6-nm FeCo films at 2 K. These results are consistent with the case of varying  $T$  from 2 to 20 K for 1.0-nm FeCo films. Moreover, the reduction of  $\gamma$  for FeCo films with  $G_{\text{xx}} > 4.22e^2/h$  may be due to the increased contribution of the side jump and/or intrinsic mechanism to the AHE [1,19,24,36]. Distinctly, there is a corresponding crossover at  $G_{\text{xx}} \sim 4.22e^2/h$  [ $R_{\text{xx}} \sim h/(4.22e^2)$ ], consistent with the thickness ( $d = 1.6$  nm) where the EEI correction to the AHE begins to disappear, shown in Fig. 4(b). This crossover could be associated with the sheet resistance  $R_{\text{xx}}$  of FeCo films at 2 K. Here we take the DOS term of the EEI correction, for example, considering the previous works [24,26,27,48–50]. While  $R_{\text{xx}} < R_{\text{Q}}$ , the EEI correction to the AHE vanishes, corresponding to the little influence of EEI on the DOS [24,48]. As  $R_{\text{xx}} \rightarrow R_{\text{Q}}/4$ , the DOS near the Fermi energy rapidly depletes due to the EEI, and a Coulomb gap

begins to open in the DOS spectrum, corresponding to EEI gradually correcting to the AHE [24,48–50]. As a result, the EEI correction to the AHE clearly presents when  $R_{xx} > R_Q/4$ .

To gain a complete understanding, it is important to point out that the disorder strength of samples can be tuned by varying thickness  $d$  or temperature  $T$ , but the effect can be quite different (see Sec. 3 and Fig. S3 in the Supplemental Material [46]; see also Refs. [51–53]). This is owing to the expectation that for EEI correction and impurity scattering, temperature-dependent (phonon and/or magnon) scatterings may also contribute to  $G_{xx}(T)$  and  $G_{AH}(T)$  while  $T$  is higher than the low-temperature limit (2 K) [54]. In particular, the intrinsic mechanism may also show temperature dependence in some systems, such as Ni films [55]. Moreover, the variation in thickness can also affect the contribution of the intrinsic mechanism, because the incomplete band structure of ultrathin films may decrease the integral of all the Berry curvatures over the whole Brillouin zone [1,9,19]. Nonetheless, the case of varying  $d$  or  $T$  can be understood because the EEI correction is closely related to the film initiatory disorder strength ( $k_F l$  at 2 K). Note that the quantum corrections in the low-temperature region would be quickly destroyed by increasing  $T$  [13]. Only strong EEI can correct to the AHE while raising  $T$  in the low-temperature region, such as 1.0–1.6-nm FeCo films with  $k_F l \sim 0.88 - 4.22$  ( $R_{xx} \gtrsim R_Q/4$ ). Additionally, the shrinking disorder strength would cause weakened EEI correction to skew scattering as  $d$  increases, resulting in reduced contribution of skew scattering to the AHE. As a result, the exponent  $\gamma$  obtained from the scaling of  $G_{AH}(T) \sim G_{xx}^\gamma(T)$  changes from  $\sim 1$  to  $\sim 0.74$  as  $d$  increases from 1.0 to 1.6 nm. In the process of raising temperature  $T$ , the possible temperature-related contribution to the AHE cannot be ignored. On the other hand, for increasing film thickness  $d$  at 2 K, the reduced disorder strength related to the EEI correction and enhanced contribution of the intrinsic mechanism would prevent skew scattering from dominating the AHE at a crossover thickness. Eventually, a crossover thickness exists in  $d = 1.6$  nm in FeCo films system [Figs. 4(b) and 6].

According to our limited knowledge,  $\gamma \sim 1$  has not been experimentally reported and is fundamentally different from the universal scaling exponent  $\gamma \sim 1.6$  in the bad metal regime

( $\sigma_{xx} < 1 \times 10^4$  S/cm) [1,33–35]. Generally, the contribution of skew scattering is proportional to the Bloch state transport lifetime and seems to dominate the AHE in nearly perfect crystals with  $\sigma_{xx} > 1 \times 10^6$  S/cm [1,4,5]. The unconventional dependence of  $\gamma \sim 1$  indicates that EEI does correct to skew scattering so that skew scattering dominates the AHE for 1.0-nm FeCo films ( $\sigma_{xx} \sim 5 \times 10^3$  S/cm) in the low-temperature region [for 1.0–1.6-nm FeCo films at 2 K ( $\sigma_{xx} \sim (5-15) \times 10^3$  S/cm)]. This result may be understood by considering that both MT [29,31] and DOS [30] terms contribute to skew scattering, but only the DOS term contributes to the side jump [26,27,32]. Importantly, the skew scattering results in a more pronounced temperature dependence and stronger dependence on impurity scattering coefficients [27]. These results suggest that the EEI correction to skew scattering overcomes the correction to the side jump for ultrathin FeCo films.

#### IV. CONCLUSION

In summary, we have systematically explored the quantum corrections to sheet conductance and anomalous Hall conductance for ultrathin single-crystal FeCo films. It is confirmed that the electron-electron interaction (EEI) corrects to sheet conductance while weak localization is absent in the low-temperature region in FeCo films. Moreover, the resulting exponent  $\gamma \sim 1$  of the AHE scaling [ $G_{AH}(T) \sim G_{xx}^\gamma(T)$ ] is observed whether the disorder strength is tuned by varying thickness  $d$  at 2 K or by changing temperature  $T$  at  $d = 1.0$  nm, indicating that EEI corrects to skew scattering and makes skew scattering dominate the AHE at low temperatures.

#### ACKNOWLEDGMENTS

We thank Professor Shiming Zhou of Tongji University for a critical reading of the manuscript and helpful discussion. This work was supported by the National Natural Science Foundation of China (Grant No. 12074157), Gansu Key Research and Development Program under Grant No. 23YFGA0008, and the Fundamental Research Funds for the Central Universities (Grant No. lzujbky-2022-kb06).

- 
- [1] N. Nagaosa, J. Sinova, S. Onoda, A. H. MacDonald, and N. P. Ong, Anomalous Hall effect, *Rev. Mod. Phys.* **82**, 1539 (2010).
  - [2] N. A. Sinitsyn, Semiclassical theories of the anomalous Hall effect, *J. Phys. Condens. Matter* **20**, 023201 (2008).
  - [3] R. Karplus and J. M. Luttinger, Hall Effect in ferromagnetics, *Phys. Rev.* **95**, 1154 (1954).
  - [4] J. Smit, The Spontaneous Hall effect in ferromagnetics I, *Physica (Amsterdam)* **21**, 877 (1955).
  - [5] J. Smit, The Spontaneous Hall effect in ferromagnetics II, *Physica (Amsterdam)* **24**, 39 (1958).
  - [6] L. Berger, Side-jump mechanism for the Hall effect of ferromagnets, *Phys. Rev. B* **2**, 4559 (1970).
  - [7] D. Yue and X. Jin, Towards a better understanding of the anomalous Hall effect, *J. Phys. Soc. Jpn.* **86**, 011006 (2017).
  - [8] Y. Yao, L. Kleinman, A. H. MacDonald, J. Sinova, T. Jungwirth, D.-S. Wang, E. Wang, and Q. Niu, First principles calculation of anomalous Hall conductivity in ferromagnetic bcc Fe, *Phys. Rev. Lett.* **92**, 037204 (2004).
  - [9] D. Xiao, M.-C. Chang, and Q. Niu, Berry phase effects on electronic properties, *Rev. Mod. Phys.* **82**, 1959 (2010).
  - [10] T. Ando, A. B. Fowler, and F. Stern, Electronic properties of two-dimensional systems, *Rev. Mod. Phys.* **54**, 437 (1982).
  - [11] G. Bergmann, Weak localization in thin films: A time-of-flight experiment with conduction electrons, *Phys. Rep.* **107**, 1 (1984).
  - [12] B. L. Altshuler and A. G. Aronov, *Electron-Electron Interactions in Disordered Systems*, edited by A. L. Efros and M. Pollak (North-Holland, Amsterdam, 1985).

- [13] P. A. Lee and T. V. Ramakrishnan, Disordered electronic systems, *Rev. Mod. Phys.* **57**, 287 (1985).
- [14] P. Wölfle and K. Muttalib, Anomalous Hall effect in ferromagnetic disordered metals, *Ann. Phys. (Leipzig)* **518**, 508 (2006).
- [15] G. Bergmann and F. Ye, Absence of a low-temperature anomaly of the anomalous Hall conductivity in thin amorphous ferromagnetic Fe films, *Phys. Rev. Lett.* **67**, 735 (1991).
- [16] A. Langenfeld and P. Wölfle, Absence of quantum corrections to the anomalous Hall conductivity, *Phys. Rev. Lett.* **67**, 739 (1991).
- [17] K. A. Muttalib and P. Wölfle, Disorder and temperature dependence of the anomalous Hall effect in thin ferromagnetic films: Microscopic model, *Phys. Rev. B* **76**, 214415 (2007).
- [18] V. K. Dugaev, A. Crepieux, and P. Bruno, Localization corrections to the anomalous Hall effect in a ferromagnet, *Phys. Rev. B* **64**, 104411 (2001).
- [19] K. Zhu, L. Wu, D. Yue, Y. Tian, and X. Jin, Anomalous Hall effect in localization regime, *Phys. Rev. B* **93**, 214418 (2016).
- [20] P. P. Mitra, R. Mitra, A. F. Hebard, K. A. Muttalib, and P. Wölfle, Weak-localization correction to the anomalous Hall effect in polycrystalline Fe films, *Phys. Rev. Lett.* **99**, 046804 (2007).
- [21] Z. B. Guo, W. B. Mi, Q. Zhang, B. Zhang, R. O. Aboljadayel, and X. X. Zhang, Anomalous Hall effect in polycrystalline Ni films, *Solid State Commun.* **152**, 220 (2012).
- [22] Y. M. Lu, J. W. Cai, Z. B. Guo, and X. X. Zhang, Unconventional scaling of the anomalous Hall effect accompanying electron localization correction in the dirty regime, *Phys. Rev. B* **87**, 094405 (2013).
- [23] T. Zhu and S. B. Wu, Thickness dependence of localization to the anomalous Hall effect in amorphous CoFeB thin films, *IEEE Trans. Magn.* **51**, 4400604 (2015).
- [24] Y. M. Xiong, P. W. Adams, and G. Catelani, Saturation of the anomalous Hall effect in critically disordered ultrathin  $\text{CNi}_3$  films, *Phys. Rev. Lett.* **104**, 076806 (2010).
- [25] S. Yang, Z. Li, C. Lin, C. Yi, Y. Shi, D. Culcer, and Y. Li, Unconventional temperature dependence of the anomalous Hall effect in  $\text{HgCr}_2\text{Se}_4$ , *Phys. Rev. Lett.* **123**, 096601 (2019).
- [26] S. Li and A. Levchenko, Temperature dependence of the anomalous Hall effect from electron interactions, *Phys. Rev. Lett.* **124**, 156802 (2020).
- [27] S. Li and A. Levchenko, Fluctuational anomalous Hall and Nernst effects in superconductors, *Ann. Phys. (NY)* **417**, 168137 (2020).
- [28] A. I. Larkin and A. A. Varlamov, *Theory of Fluctuations in Superconductors* (Clarendon, Oxford, 2005).
- [29] K. Maki, The critical fluctuation of the order parameter in type-II superconductors, *Prog. Theor. Phys.* **39**, 897 (1968).
- [30] E. Abrahams, M. Redi, and J. Woo, Effect of fluctuations on electronic properties above the superconducting transition, *Phys. Rev. B* **1**, 208 (1970).
- [31] R. S. Thompson, Microwave, flux flow, and fluctuation resistance of dirty type-II superconductors, *Phys. Rev. B* **1**, 327 (1970).
- [32] H. Fukuyama, H. Ebisawa, and T. Tsuzuki, Fluctuation of the order parameter and Hall effect, *Prog. Theor. Phys.* **46**, 1028 (1971).
- [33] T. Miyasato, N. Abe, T. Fujii, A. Asamitsu, S. Onoda, Y. Onose, N. Nagaosa, and Y. Tokura, Crossover behavior of the anomalous Hall effect and anomalous Nernst effect in itinerant ferromagnets, *Phys. Rev. Lett.* **99**, 086602 (2007).
- [34] S. Onoda, N. Sugimoto, and N. Nagaosa, Quantum transport theory of anomalous electric, thermoelectric, and thermal Hall effects in ferromagnets, *Phys. Rev. B* **77**, 165103 (2008).
- [35] S. Sangiao, L. Morellon, G. Simon, J. M. De Teresa, J. A. Pardo, J. Arbiol, and M. R. Ibarra, Anomalous Hall effect in Fe (001) epitaxial thin films over a wide range in conductivity, *Phys. Rev. B* **79**, 014431 (2009).
- [36] P. J. Wang, P. Chen, Y. Z. Wang, Z. Y. Lian, P. Liu, X. L. Li, Y. Miao, and C. X. Gao, Sign change of competing contributions to the side jump by impurity, phonon, and magnon scattering, *Phys. Rev. B* **107**, 094418 (2023).
- [37] F. Tang, T. Parker, G.-C. Wang, and T.-M. Lu, Surface texture evolution of polycrystalline and nanostructured films: RHEED surface pole figure analysis, *J. Phys. D Appl. Phys.* **40**, R427(R) (2007).
- [38] T. Sourmail, Near equiatomic FeCo alloys: Constitution, mechanical and magnetic properties, *Prog. Mater. Sci.* **50**, 816 (2005).
- [39] N. Ashcroft and N. Mermin, *Solid State Physics* (Saunders College, Philadelphia, 1976).
- [40] H. Ibach and H. Lüth, *Solid-State Physics: An Introduction to Principles of Materials Science* (Springer-Verlag, Berlin, 1996).
- [41] D. Hou, Y. Li, D. Wei, D. Tian, L. Wu, and X. Jin, The anomalous Hall effect in epitaxial face-centered-cubic cobalt films, *J. Phys.: Condens. Matter* **24**, 482001 (2012).
- [42] C. R. Tellier and A. J. Tossier, *Size Effects in Thin Films* (Elsevier, Amsterdam, 1982).
- [43] B. L. Altshuler, A. G. Aronov, and P. A. Lee, Interaction effects in disordered Fermi systems in two dimensions, *Phys. Rev. Lett.* **44**, 1288 (1980).
- [44] Y.-J. Zhang, K.-H. Gao, and Z.-Q. Li, Crossover of electron-electron interaction effect in Sn-doped indium oxide films, *Appl. Phys. Lett.* **106**, 101602 (2015).
- [45] S. Kobayashi and F. Komori, Experiments on localization and interaction effects in metallic films, *Prog. Theor. Phys. Suppl.* **84**, 224 (1985).
- [46] See Supplemental Material at <http://link.aps.org/supplemental/10.1103/PhysRevB.109.144416>. Section 1 presents  $\ln T$ -type dependence of  $R_{\text{AH}}$  and  $G_{\text{AH}}$  of FeCo films at low temperatures. Section 2 displays  $-\sigma_{\text{AH}}$  vs  $\sigma_{xx}$  for 1.0–43.8-nm FeCo films, indicating that the competing scattering still exists and is noticeable even for 2.0-nm FeCo films with  $\sigma_{xx} \sim 2 \times 10^4 \Omega^{-1} \text{cm}^{-1}$ . Section 3 shows  $-\sigma_{\text{AH}}$  vs  $\sigma_{xx}$  for 1.0–43.8-nm FeCo films, revealing the limitations of the general scaling of  $-\sigma_{\text{AH}}$  vs  $\sigma_{xx}$  while including the changes in both thickness and temperature.
- [47] D. C. Licciardello and D. J. Thouless, Constancy of minimum metallic conductivity in two dimensions, *Phys. Rev. Lett.* **35**, 1475 (1975).
- [48] V. Yu. Butko, J. F. DiTusa, and P. W. Adams, Coulomb gap: How a metal film becomes an insulator, *Phys. Rev. Lett.* **84**, 1543 (2000).
- [49] V. Y. Butko and P. W. Adams, Quantum metallicity in a two-dimensional insulator, *Nature (London)* **409**, 161 (2001).
- [50] M. Pino, A. M. Somoza, and M. Ortuno, Quantum Coulomb gap in low dimensions, *Phys. Rev. B* **86**, 094202 (2012).
- [51] Y. Tian, L. Ye, and X. Jin, Proper scaling of the anomalous Hall effect, *Phys. Rev. Lett.* **103**, 087206 (2009).

- [52] D. Hou, G. Su, Y. Tian, X. Jin, S. A. Yang, and Q. Niu, Multi-variable scaling for the anomalous Hall effect, *Phys. Rev. Lett.* **114**, 217203 (2015).
- [53] J. Xu, L. Wu, Y. Li, D. Tian, K. Zhu, X. Gong, and X. Jin, The anomalous Hall effect in epitaxial Fe(110) films grown on GaAs(110), *Sci. Bull.* **60**, 1261 (2015).
- [54] G. Su, Y. Li, D. Hou, X. Jin, H. Liu, and S. Wang, Anomalous Hall effect in amorphous  $\text{Co}_{40}\text{Fe}_{40}\text{B}_{20}$ , *Phys. Rev. B* **90**, 214410 (2014).
- [55] L. Ye, Y. Tian, X. Jin, and D. Xiao, Temperature dependence of the intrinsic anomalous Hall effect in nickel, *Phys. Rev. B* **85**, 220403(R) (2012).